Numerical Simulation of Transient Aerodynamic Phenomena during Crosswind flow on High Speed Train

o Rakshita Bagherwal,Hokkaido Univ.,N13,W8,Kita-ku,Sapporo,Hokkaido 060-0808, rb5628@gmail.com
Jun Ikeda, Kobe Univ.,1-1, Rokkodai-Cho,Nada-Ku,Kobe-Shi,Hyogo 657-8501,jun_ikeda@port.kobe-u.ac.jp
Nobuyuki Oshima, Hokkaido Univ., N13,W8,Kita-ku, Sapporo, Hokkaido 060-0808,oshima@eng.hokudai.ac.jp
Makoto Tsubokora, Kobe Univ., 1-1, Rokkodai-Cho,Nada-Ku,Kobe-Shi,Hyogo 657-8501,tsubo@tiger.kobe-u.ac.jp

This paper presents a large eddy simulation method based on fully unstructured finite volume method, and unsteady aerodynamic response of a high-speed train vehicle subjected to transient crosswind was investigated. First, the method was validated for train model in three static aerodynamic conditions with different crosswinds; showing good agreement of aerodynamic forces and moments with wind-tunnel data, as provided in EN-14067-6. Then, the method was applied to transient crosswind situation: a sinusoidal perturbation gust representing a gradually varying crosswind yaw angle, in range typical with real trains. Typical transient responses of aerodynamic forces and moments such as increase with yaw angles, phase responses were observed, and their dependence on shape and amplitude of wind perturbation was discussed. Consequentially, application and validity of large eddy simulation was illustrated with reference to train vehicles, esp. as this detailed aerodynamic force results are difficult to be obtained from conventional wind tunnels.

Introduction:

The effect of crosswinds is one of the most critical problems connected to the train safety and stability. A train travelling through a natural turbulent crosswind is surrounded by a complex flow field which leads to a series of steady and unsteady aerodynamic forces and moments. These aerodynamic loads may influence the vehicle dynamic behaviour seriously, and in presence of strong crosswinds, serious accidents may happen. These crosswind related accidents date back to the 19th century, and still occur today. One accident is shown in fig1.1, showing the overturned first two cars of an electric multiple unit in Switzerland in 2007 (during the winter storm Kyrill due to high wind speeds of 55 mph. It represents the most common crosswind accident type for rail vehicles, which is overturning about one of the rails.

Fig.1.1 Train accident in Switzerland due to strong winds,2007: source[(1)]

With rapid enhancement in train running speeds and energy efficiency, during the last few decades, and a consequential reduction in weight of the rail vehicles, the crosswind stability has become even more important for the running stability and riding comfort of the vehicle. Further, the traction layout of passenger trains, not only for high-speed trains, but also for regional trains, is changing from loco-hauled trains to multiple units with distributed traction. Since the aerodynamic loads are the most critical on the leading vehicle of a train, the weight change from a locomotive engine- as the leading and heaviest vehicle of a locomotive driven train - to a multiple unit vehicle increases the demand for crosswind stability of trains.

Unsteady crosswind and the related phenomena have become a major concern in comparison to steady state conditions. A rail vehicle can be subjected to various unsteady wind situations in everyday operation, including gusts in open field, gust-like wind conditions due to changes near the track, eg Vegetation, tunnels, as well as effects of passing vehicles. Bridge and embankments involve even higher wind speeds, due to atmospheric boundary layer and accelerated flow at the top of embankment. At tunnel exits, wind speeds drastically increase. As crosswind stability is significant safety issue, detailed information about the behaviour of the vehicle in crosswinds is very important. Different studies have been undertaken in the past for evaluating the impact that the vehicle movement simulation has on the crosswind loads on trains. Since, the 1980s, the problem was approached from an experimental perspective and several moving model test campaigns were carried out [(2), (3)]; a large bibliography exists on railway vehicle aerodynamics and many authors have mentioned the importance of a large number of factors ,e.g. Baker and Humphreys (1996) [(4)] , Schetz (2001) [(5)] and Baker et al. (2004) [(6)].But the effects on load of most of these factors ,like wind velocity profile, turbulence length, intensity etc. are very difficult to assess. Also, using measurements including field experiments with a moving rail vehicle at the risk of overturning is fundamentally difficult for safety and economic reasons. Therefore, simulations represent a necessary and important tool. Large eddy Simulations (LES), is a promising tool for the estimation of the transient aerodynamic forces acting on a vehicle. Large-Eddy simulation can reproduce 3-dimensional unsteady flow structures around the road vehicles and provide unsteady aerodynamic data which are difficult to obtain through conventional measurements.

However, before quantitative conclusions can be drawn based on numerical results, it is essential to assess the level of accuracy of CFD when applied to vehicles in motion. Such a comparison

requires detailed and reliable experiment data. We have used European Standard EN-14067-6 :2010(7), as the reference standardisation document, which being the most important regulation document related to high Speed trains, deals with crosswind stability of rail vehicles and describes assessment methods for crosswind stability. An ICE 3 model is one available model, which is a streamlined high-speed train model. The reference setup used for crosswind assessments of trains in wind tunnel testing is standardised single track ballast and rail(STBR).

As the objective of this research, we apply our High Performance Computing (HPC) LES based numerical method for estimating the unsteady aerodynamics of a streamlined high-speed rail vehicle ICE3 in multiple cross wind related phenomena in which conventional wind tunnel or on-site measurements are difficult to use. The computational code used in the numerical method was based on unstructured finite volume method to treat a scaled model with very complicated geometry. To satisfy the demands of such a high computational cost, the computational code had been optimized for a massively parallel processor.

In this study, firstly, validation cases were performed using HPC-LES, by comparing steady simulation result with wind tunnel experimental data (EN14067-6) for three crosswind yaw angle scenarios on a high-speed train model ICE3 with complicated geometry. The three-dimensional flow-structures were observed and compared in detail and averaged aerodynamic forces were compared with the wind tunnel measurements (EN-14067-6) to prove the fundamental validity of the method. Afterwards, the cases of transient crosswind (case of time-varying crosswind yaw angles) were performed on the ICE3 geometry model to obtain time dependent aerodynamic forces and moments. We qualitatively discuss the resulting three-dimensional unsteady flow structures around the vehicle, and their relationship with crosswind gust modelling. Finally, importance of the unsteady aerodynamics and application of LES in time varying crosswind condition have been discussed.

Numerical Methods:

2.1. Target Vehicle and Base

The streamlined ICE3 train 1:25 scaled model is used for our study. The ICE3 represents the high-speed, streamlined trains, and the geometry is that of the reference train in the EN-14067-6. The surface geometry of the vehicle body was precisely reproduced from computer-aided design data for a real scale model, including the bogies and inter-car gaps, fig.2.1.1. The critical details on the train are: a long, streamlined nose and a smooth round shaped roof. The first vehicle is the most critical vehicle to crosswind, therefore considered in the study. The half vehicle is modelled downstream in the ICE3 for accurate description of inter vehicle gaps according to EN norm. The coefficients are calculated for the most critical vehicle, i.e. the first vehicle.

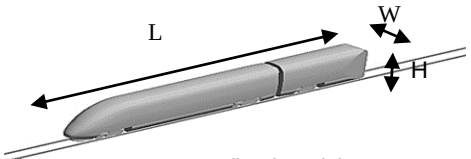

Fig. 2.1.1: ICE3: streamlined model

The dimensions of the train model with the base are 1.529m(length) ×0.118m(width) ×0.159m(height). The surrounding base geometry is modelled as single-track ballast and rails(STBR), according to description in EN-14067-6. This is the standardized 1m ballast and rail configuration, essentially a standardized simplified model (the sleepers are not modelled), fig.2.1.2. The underbody flow field in this model is fairly represented in this configuration by providing appropriate blockage to the air flow.

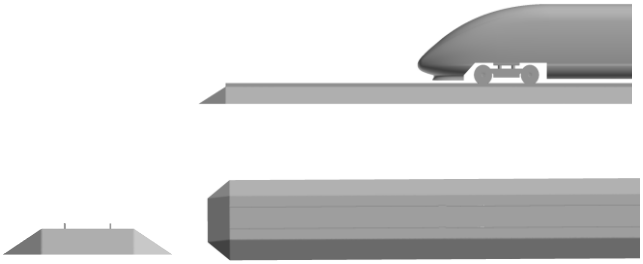

Fig.2.1.2: Standard Track Base and Rail Geometry

The size of the computational domain is 10L,20 W and 10 H for streamwise, span-wise, and normal-wall directions, respectively, as illustrated in fig.2.1.3

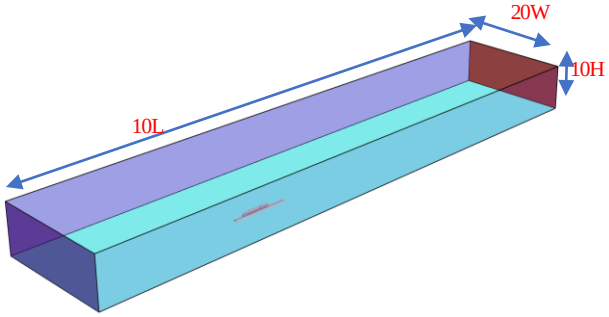

Fig. 2.1.3: Computational domain

The size of the domain is big enough to satisfy the requirement of EN14067-6:2010. The train and track are aligned parallel to the sides of the domain. The front and left side are used as inlets, whereas the right side and rear are outlets. The same domain and mesh setup could be used for any wind angles (both βw and β) just by changing the boundary conditions. This considerably reduces the mesh generation time for different yaw angles. To avoid the possible blockage effect, the cross-sectional size is set to be relatively larger, as compared to the wind tunnel facilities; with blockage ratio with respect to vehicle cross-section less than 1%.

2.2 Governing Equations:

The incompressible Newtonian fluid is assumed, and the governing equations are given by the spatially filtered continuity and Navier-Stokes equations, as indicated below. Because of high

Reynolds Number turbulence around the vehicle, a sub-grid-scale (SGS) stress is used to capture a relatively high wave number turbulence.

$$\frac{\partial \bar{u}_i)}{\partial x_i} = 0$$

$$\frac{\partial \bar{u}_i}{\partial t} + \frac{\partial}{\partial x_j}\bar{u}_i\bar{u}_j = \frac{-\partial \bar{P}}{\partial x_i} + 2\frac{\partial}{\partial x_j}(v + v_{SGS})\bar{S}_{ij}$$

$$\bar{S}_{ij} = \frac{1}{2}\left(\frac{\partial \bar{u}_j}{\partial x_j} + \frac{\partial \bar{u}_i}{\partial x_j}\right)$$

$$\bar{P} = \frac{\overline{p}}{\rho} + \left(\overline{u_i u_i} - \bar{u}_i\,\bar{u}_i\right)/_3$$

Where u, P, v and ρ are the velocity, pressure, kinetic viscosity, and density, respectively. The SGS eddy viscosity is modelled following Smagorinsky as,

$$v_{SGS} = (C_s f_s \Delta)^2 \sqrt{\bar{s}_{ij}\bar{s}_{ij}}$$

In which Δ is the volume of numerical elements and the model coefficient is given as Cs=0.15 in this study. The following Van-Driest type damping function is adopted:

$$f_s = 1 - \exp\left(-\frac{y^+}{26}\right)$$

2.3 Computational conditions

Discretization

The governing equations are discretized by the vertex-centred unstructured finite volume method. In the finite volume method, the governing equations are based on the following conservation equation in integral form.

$$\frac{\partial}{\partial t}\int_\Omega \rho\,\emptyset d\Omega + \int_S \rho\,\mathbf{v}.\mathbf{n}\emptyset dS = \int_S \Gamma\, grad\emptyset.\mathbf{n}dS$$

where the second term on the left is the convective term and the right is the diffusion term. All dependent variables are defined on each vertex of numerical elements and a virtual control volume is constructed around the target vertex. Governing equations are integrated over the volume. The central finite difference scheme with the second order accuracy is basically applied to spatial discretization. The 2nd order central finite difference is mainly used for spatial discretization,5% 1st order upwind difference is blended to the 2nd order central finite difference when discretizing the convective term to eliminate numerical oscillations especially at region where relatively coarse grid is allocated. Time integration is based on the Euler implicit method. Fractional step method is used for pressure-velocity coupling, we used ICCG to solve the pressure-poisson equations.

2.4 Grid Resolution

A total of about 66 million tetrahedron elements were used to cover the entire computational domain. The solid surface (ICE3) was reproduced by triangular meshes with a spatial resolution of a few millimeters. The cell sizes near the train and STBR should be very fine so that the small eddies, flow separations and boundary layer phenomena can be captured. Large vortices in the far wake can be resolved even with a bigger cell size. The cell sizes and regions are defined through the size boxes, as in fig.2.4.1, and fig.2.4.2

level	Domain name	%of base	Absolute value(1:25)
1	vehicle	5	2mm
2	Near (vehicle and base)	10	5mm
3	Near wake	20	12mm
4	Far wake	100	45mm

Fig 2.4.1: description of mesh parameters with size boxes definition

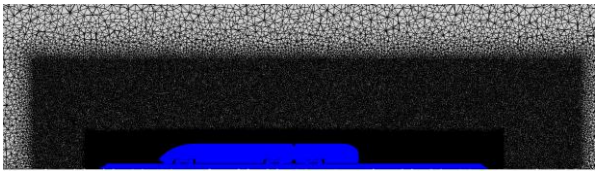

fig.2.4.2: Mesh resolution near the vehicle and wake definition

2.5 Boundary Conditions

In this study, the focus was the train vehicle aimed straight ahead subjected to gusty or continuously fluctuating crosswinds, as schematically shown in fig.2.5.1. The flow field was reproduced in CFD by fixing the coordinates on the vehicle, and the crosswind region was convected downstream at the same speed as the assumed vehicle velocity. To achieve a convective crosswind, we imposed the crosswind's lateral velocity profile on the side of the computational domain and it was transported downstream at the same speed as the main inlet velocity (Tsubokura et al., 2008b). The Reynolds number with respect to the main incoming flow U (38m/s) and the vehicle length L was 0.3 million. For the accuracy of the outlet condition, we attached an additional layer consisting of prism elements at the exit of the domain to align the grid lines with the mean velocity direction.

On the surfaces of the car body, a solid wall condition is adopted. The assumed log-law profile is directly applied to the instantaneous velocity field for estimating the surface friction. On the floor, free slip condition is applied to prevent the boundary layer from developing. The ceiling of the numerical domain is supposed to be free-slip on the surface.

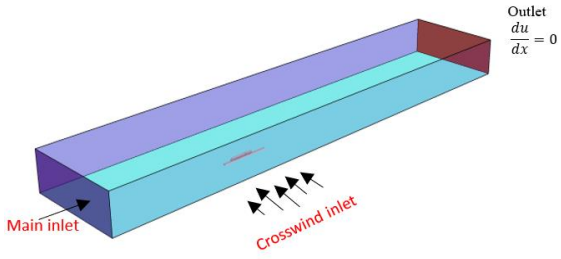

Fig.2.5.1: Inlet and outlet Boundary conditions

Analysis Software

The computational code adopted is the FrontFlow/red-Aero, which was optimized for HPC, and its accuracy has been tested on

numerous unsteady simulations studies. All numerical simulations were conducted on an ITO-a (Kyushu-University) supercomputer. Twenty computational nodes (720 CPUs) were used to calculate each time-step in real seconds. The simulations were time-integrated by the Euler implicit method with a time increment of dt=9x10-6 for precise prediction of the unsteady aerodynamics. The time increment was determined to give CFL numbers of less than 1 for the Euler implicit method.

3.1 Validation

The numerical method was validated for steady-aerodynamics analysis at various yaw angles, viz 0, 5 and 10 degrees, and the averaged aerodynamic forces and moments acquired numerically were compared with the standardized wind tunnel data provided in EN14067-6:(2010).The simulation results are being compared with EN results for yaw angles, 0,5,10 degrees in the graphs shown in fig.3.1.1 attached. The Force coefficients being defined as

Non-dimensional force coefficient based on A_0	$c_{Fi} = \frac{2 \cdot F_i}{\rho \cdot v^2 A_0}$, i = x, y, z
Non-dimensional moment coefficient based on A_0 and d_0	$c_{Mi} = \frac{2 \cdot M_i}{\rho \cdot v^2 A_0 d_0}$, i = x, y, z

The drag and side forces coefficients showed a very good agreement with discrepancies less than 8%, the lift force coefficients showed a higher discrepancy less than 17%. One possible explanation for the higher discrepancy in lift forces is the differences in the accuracy of model geometry between the present LES and the wind tunnel experiments. In the present LES, the train geometry was modelled very accurately, esp. the volumes where flow exists; this included the multiple open pillar structures entering the vehicle geometry and the fine details in underframe, i.e. bogies, whereas in the wind tunnel measurement, a completely wrapped model with not much detailing to pillars or underframe was used, this possibly caused the discrepancy in lift force values. There are considerable discrepancies at higher yaw angles in side force, as being influenced by the differences in blockage between wind tunnel experiment and the present LES. From the comparison, it is clear that as the yaw angle increases, the coefficients increase. Here the simulations are done for yaw angles less than 50 degrees, if we look in the EN results from EN14067-6(9), after 50degree yaw angle, the coefficients drop. The surface pressure distributions on the train vehicle for cases of yaw angles as 0, 5 and 10 degrees are shown in fig.3.1.2

We can observe the frontal stagnation point being shifted accordingly as the wind inflow direction. In fig 3.1.3, we show the lee side vortex (Pressure iso surfaces-using q criterion) for all the three cases, the vector field shows strongest vortex field near the ground and near the roof for 10 degrees yaw angle case, the strength of the vortex grows with yaw angle. This strong vortex causes lower Pressure, and consequently, higher side and lift force. Generally, the LES results show good agreement with the experimental data.

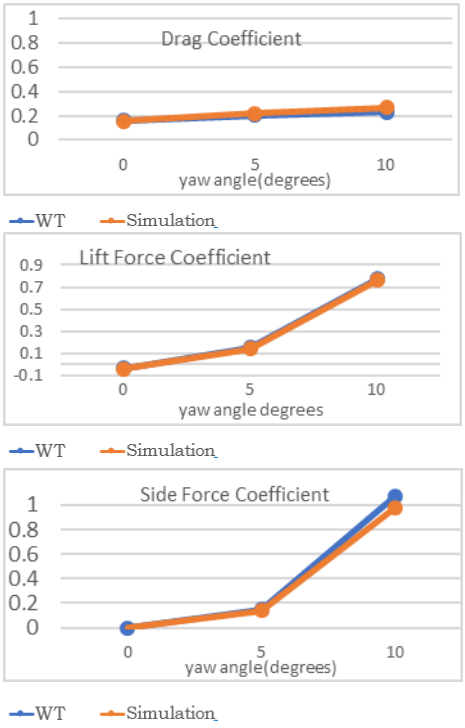

Fig.3.1.1:Aerodynamic forces coefficients versus yawing angle in static yaw angle crosswind profiles

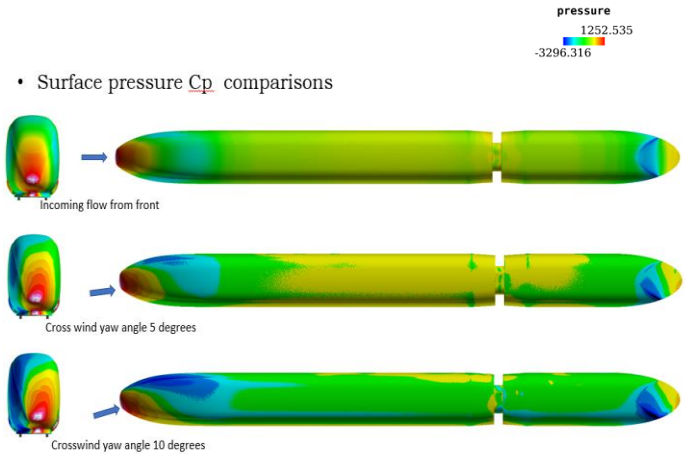

Fig.3.1.2: Surface Pressure Profiles: variation with crosswind yaw angle

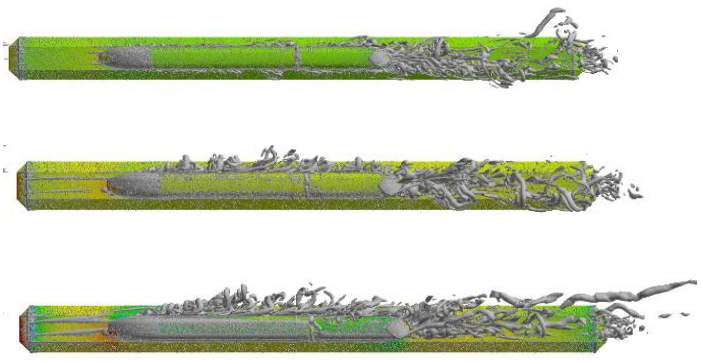

Fig.3.1.3: surface pressure iso -surfaces of vorticity magnitude :(q-criterion):in order from top to bottom: 0° yaw angle, 5° yaw angle, 10 ° yaw angle

3.2 Transient Simulation:

Continuous Yaw angle change

To investigate the effect of unsteady ambient crosswind flow on the vehicle aerodynamics, and especially its aerodynamic response to wind gust shapes, we overlapped the sinusoidal transverse velocity profiles on the main incoming flow. The crosswind profiles were imposed as an inlet/outlet boundary condition on both sides of the computational domain, as shown in Fig.2.1.3. They are expressed as

$$v = Asin2\pi(\frac{x}{\lambda} - ft)$$

Because the sinusoidal profile travels at the same velocity as the inlet velocity, the frequency is given by

$f = \frac{U}{\lambda}$.

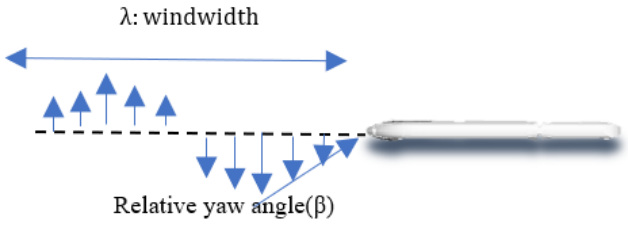

Fig 3.2.1: overview of sinusoidal crosswind imposed

In the present study, an initial wavelength of 10L of crosswind was assumed, and a continuous yawing angle change with respect to the incoming flow was varied between +6 degrees to -6 degrees for a general sinusoidal crosswind case. With incoming velocity of 38m/s and vehicle length 1.02m, the maximum applied lateral(y) velocity relative to the vehicle reached an Amplitude of about 4 m/s corresponding to maximum yaw. The wind comes in after t=0.18 s, this was specifically implemented for appropriate flow development. The sinusoidal transversal velocity profile imposed on the incoming flow and its wavelength and amplitude are summarized in Fig.3.2.1

The time series of the aerodynamic forces and moments in the case are plotted in the fig.3.2.2-3, all units are in SI units. The reference crosswind profile is also indicated. The sinusoidal aerodynamic responses of the side force as well as the yaw and roll moments are evidently observed, while their phases are slightly shifted with respect to the crosswind velocity. The roll moment variation with respect to time is also shown. For side-wind stability, the roll moment with respect to lee Rail (downstream) is responsible for wheel unloading. We can see that the vehicle went straight ahead through the sinusoidal crosswind and drag, lift is relatively perturbed, with their sinusoidal responses are unclear. The drag coefficient, important only for energy considerations and not safety, evidently is not affected to a large extent, with only slight variations.

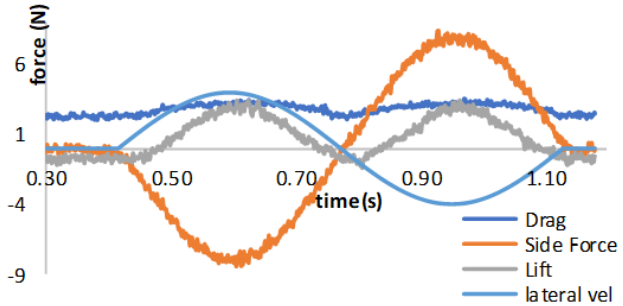

Fig.3.2.2 The time series of the aerodynamic forces (N) and lateral velocity (m/s)

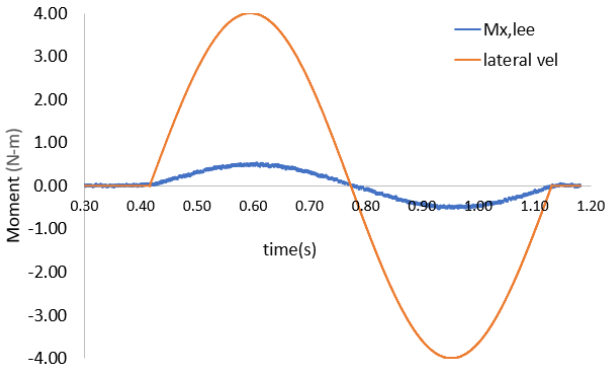

Fig.3.2.3 The time series of the roll moment (N-m) across Lee rail with lateral velocity (m/s)

For better understanding of the responses of side force and yaw moment's sinusoidal behaviour, we visualised snapshots of flow structures around the vehicle at different times, and are described in fig.3.2.4, identical observations, but in the opposite direction were obtained for the negative half cycle.

1) Surface Pressure contours (top view):, just before vehicle front approaches crosswind,

2) Surface Pressure contours (top view): vehicle front has approached positive crosswind amplitude (peak yaw angle)

3) Surface Pressure contours (top view): vehicle has traversed half wavelength crosswind

Fig.3.2.4: Surface pressure contours: top view

From the surface pressure profiles over the vehicle body, we see that as the crosswind grows over time, i.e. with increase in yaw angle, the position of pressure stagnation point moves farther on the leeward side for the positive and negative wind cycle.

On the windward side, there is a large stagnation region at the nose where the crosswind impinges on the train body, followed by a region of relatively milder pressure over most of the remaining surface. Both the underside of the train and its top surface are regions of low pressure. We could see at the leeward side, negative pressure existed due to the existence of a relatively strong rotating vortex, compared to windward side. The

existence of the lower pressure region on the leeward side of the train can explain the increased side force and roll moment.
As we observe the iso -surface of vorticity magnitude fig.3.2.5 at different stages of rushing-in, we can observe the typical flow structures, mainly the vortices generated near the nose, on leeward side, increasing in strength with the increasing yaw angle, as this directly relates to increase in the side force with yaw angle. As the yaw angle increases, higher number vortices are generated at the leeward side, which eventually cause a lower pressure region on the side, increasing the roll moment.

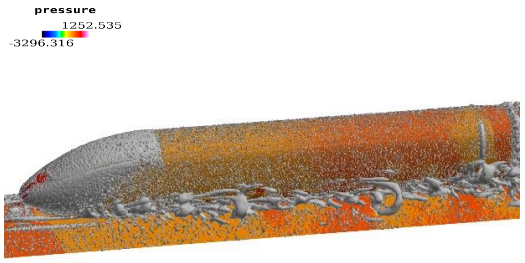

Fig.3.2.5 (a).vehicle just entered crosswind region

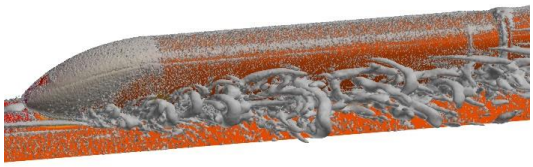

Fig.3.2.5 (b) Vehicle approached peak positive crosswind velocity
Fig.3.2.5 (a),(b)showing iso-surfaces of vorticity magnitude(q-criterion) at different time steps

As the crosswind flow across the vehicle grows for the first sinusoidal half wind wavelength, development of the side separation could be observed, evidently the highest when the sinusoidal wave crosswind velocity reaches its amplitude at front of the vehicle. From fig.3.2.6, we can see that this separation grows from the nose and extends over much of its surface from aft of the nose till the back end of the train. Perhaps, this also enhanced low pressure region over roof which could be observed from the surface pressure snapshots for different time periods.

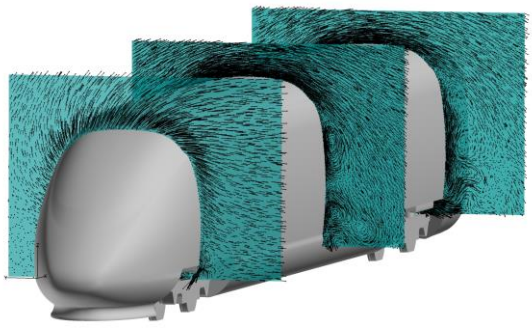

Fig.3.2.6 Velocity contours along the train's cross-section at the time when train approaches peak crosswind (length l is defined originating from nose of the train)

4. Conclusions

An LES method for the unsteady aerodynamics of High Speed Rail vehicles was developed on the basis of a fully unstructured finite volume method, and the unsteady aerodynamic response of a road vehicle subjected to sinusoidal crosswind was investigated.

The method was validated by comparing uniform crosswind simulation results with Standardised European Standard EN14067-6 Railway applications–Aerodynamics: Requirements, test procedures for cross wind assessment; the results showed good agreement.

In the continuous sinusoidal yawing case, all components of forces and moments showed more or less sinusoidal responses, i.e. similar to the wind gust model used, but their phases were observed to be shifted. Detailed flow structures were visualised, separations at the leeward side (downstream) were observed. Considering long period of time because of an elongated geometry model, using large -scale computational grids, LES was optimized for massive parallel processing.

Finally, the developed unsteady model was investigated for only one case, but further cases of crosswind gust variations including altering frequencies, wind profile etc. can be simulated in the context of observing aerodynamic force variation and stability, for crosswind safety of train vehicles.

References and bibliography:

(1) E. Andersson, J. Häggström, M. Sima, and S. Stichel, Assessment of train-overrturning risk due to strong cross-winds. Proc. IMechE F: J. Rail Rapid Transit 218 (2004), pp. 213–223

(2) J.P.Howel. Aerodynamic Response to Maglev train models to crosswind gust. Journal of Wind Engineering and Industrial Aerodynamics

(3) A. Carrarini . Reliability based analysis of the crosswind stability of railway vehicles

(3) CEN - EN 14067-6. Railway applications - Aerodynamics - Part 6: Requirements and test procedures for cross wind assessment

(4) C. Baker, N. Humphreys. Assessment of the adequacy of various wind tunnel techniques to obtain aerodynamic data for ground vehicles in cross winds

(5) J. Schetz. Aerodynamics of high-speed trains. Ann. Rev. Fluid. Mech., 33 (2001), pp. 371-414

(6) C. Baker, et al. Measurements of the crosswind forces on trains. J. Wind Eng. Ind. Aerodyn., 92 (2004), pp. 547-563

(7) Mikael Sima, Sandor Eichinger et al. Computational fluid dynamics simulation of rail vehicles in crosswind: Application in norms and standards. Proceedings of the Institution of Mechancal Engineers, Part F; Journal of rail and Rapid Transport

(8) Nachiyappan Venkatasalam. Crosswind Assessment of trains on different ground configurations Bombardier KTH Engineering Sciences

(9) A. Bouferrouk1, D. Hargreaves and H. Morvan, CFD Simulations of Crosswind Impinging on a high-speed Train Model

(10) Robinson, C.G., Baker, C.J., The Effect of Atmospheric Turbulence on Trains, Wind. Eng. Industrial Aerodynamic, 34, 1990, 251-27

(11) Makoto Tsubokora, Takuji Nakashima, Masashi Kitayama, Large Eddy Simulation on the unsteady aerodynamic response of a road vehicle in transient crosswinds. International journal of heat and fluid flow 31(2010) 1075-1086

(12) Chris Baker, Federico cheli, Alexander Orellano. Cross-wind effects on road and rail vehicles. International Journal of vehicle mechanics and Mobility volume 47,2009

(13) Sufiah Mohd Salleh et al. Aerodynamics characteristics around simplified High Speed Train Model under effect of crosswinds.ARPN, Journal of Engineering and Applied Sciences 2017,vol.12